3D-Printed Strain-Gauge Micro Force Sensors

Juntian Qu, *Student Member, IEEE*, Qiyang Wu, *Student Member, IEEE*, Tyler Clancy, Qigao Fan, *Member, IEEE*, Xin Wang, *Member, IEEE*, and Xinyu Liu, *Member, IEEE*

***Abstract*—This paper presents the development of 3D-printed micro force sensors with micronewton sensing resolutions. Two representative 3D printing techniques, fused deposition method (FDM) and stereolithography (SLA), are utilized to establish polymeric micro sensor structures with a resolution down to 300 μm. Two types of 3D-printed strain-gauge force sensors have been designed aiming at different force measurement ranges (0-2.5 mN and 0-120 mN) with micronewton force sensing resolutions (4.3 μN and 56 μN, respectively). As a proof-of-concept demonstration, the two 3D-printed force sensors are used in custom-made mechanical characterization systems for measuring Young's moduli of polydimethylsiloxane (PDMS) samples at different crosslinking levels. The experimental technique presented here could empower rapid prototyping of high-performance force sensors utilizing consumer-level 3D printers, and will significantly boost the flexible design and customization of force-sensing systems with a variety of design requirements.**

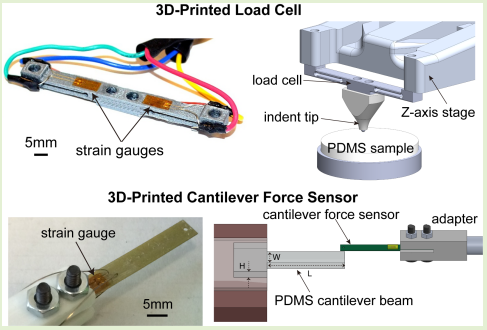

***Index Terms*—3D printing, fused deposition method (FDM), stereolithography (SLA), micro force sensor, rapid prototyping, mechanical characterization.**

I. Introduction

THREE-DIMENSIONAL printing (3DP), a rapid and economical technology in manufacturing, has attracted much attention in various fields in recent years. In contrast to traditional subtractive manufacturing methods where one starts with a big block of material and 'carve' it to the desired shape, 3DP is an additive method that builds up objects layer by layer. Generally, there are two types of 3DP principles for printing polymeric parts: fused deposition modeling (FDM) [1], [2] and stereolithography (SLA) [3], [4]. FDM operates by deposition of filament through a heating nozzle to build up the object layer by layer, while SLA adopts photocurable pre-polymer as the starting material and stiffens the material in pre-designed 3D shapes through UV light scanning. With its prominent capabilities of reducing prototyping turnaround time and being low-cost at the same time, 3DP has been employed in a broad range of research and development fields such as medical science [5], aerospace industries [6], and bioengineering [7].

High design flexibility is a unique feature of 3DP, which benefits many activities by allowing researchers to create complex shapes without the need to consider many constraints raised by conventional machining. Time and cost efficiency is another significant advantage of 3DP. In contrast to conventional manufacturing methods which may need the assembly of several parts, 3DP is able to create an assembled object from a single printing, which greatly reduces the complexity and time of the manufacturing process. Various commercially-available, inexpensive 3D printers, along with their easy-to-master design tools, also make 3DP available to almost anyone who are interested in rapidly converting their designs into real prototypes.

3DP has also been widely used in the development of various types of sensors such as liquid sensors [8], ultrasonic sensors [9], tactile sensors [10], biosensors [11], optical sensors [12], capacitive sensors [13], strain sensors [14], [15], electrochemical sensors [16], and soft electronic sensors [17]. Representatively, Muth *et al.* [15] created a stretchable strain sensor using 3DP to directly integrate sensing materials into

Manuscript received November 9, 2019; revised February 3, 2020; accepted February 7, 2020. Date of publication February 28, 2020; date of current version June 4, 2020. This work was supported in part by the National Sciences and Engineering Research Council of Canada under Grant RGPIN-2017-06374 and Grant RGPAS 2017-507980, and in part by the University of Toronto. This is an expanded article from the 2016 International Conference on Manipulation, Automation and Robotics at Small Scales (MARSS). The associate editor coordinating the review of this article and approving it for publication was Prof. Sheng-Shian Li. *(Juntian Qu and Qiyang Wu contributed equally to this work.) (Corresponding author: Xinyu Liu.)*

Juntian Qu, Qiyang Wu, and Xinyu Liu are with the Department of Mechanical and Industrial Engineering, University of Toronto, Toronto, ON M5S 3G8, Canada, and also with the Department of Mechanical Engineering, McGill University, Montreal, QC H3A 0C3, Canada (e-mail: xyliu@mie.utoronto.ca).

Tyler Clancy is with Ciena Corporation, Ottawa, ON K2K 0L1, Canada.

Qigao Fan is with the Department of Mechanical and Industrial Engineering, University of Toronto, Toronto, ON M5S 3G8, Canada, and also with the College of Internet of Things Engineering, Jiangnan University, Wuxi 214122, China.

Xin Wang is with the Department of Mechanical and Industrial Engineering, University of Toronto, Toronto, ON M5S 3G8, Canada, and also with the Department of Mechanical and Aerospace Engineering, Jilin University, Changchun 130012, China.

Digital Object Identifier 10.1109/JSEN.2020.2976508

highly stretchable polymer matrices, which is difficult for conventional manufacturing processes. They demonstrated the use of this sensor for hand posture detection. Willis *et al.* [12] fabricated customized optical elements with embedded optical sensors using 3DP, in which all the structures were printed together rather than assembled one by one. Leigh *et al.* [13] developed a conductive thermoplastic composite for 3DP and used this material to fabricate low-cost strain-gauge and capacitive sensors. This conductive composite can be co-printed with conventional thermoplastics, which allows sensors to be embedded in plastic objects without assembly.

Force sensors play a critical role in many fields such as robotics and manufacturing. By measuring the deformation of a force sensing flexure under an applied force, a force sensor can output an electrical signal like voltage that is proportional to the applied force. For instance, strain-gauge based force sensors have been employed in robotic micromanipulation systems [18] and grasping/interaction force sensing tasks [19]. Basides the conventional force sensor designs, researchers have also applied 3DP to force sensor fabrication. 3DP enables rapid and low-cost protyping of a custom-made force sensor design for a specific system and allows a user to conduct multiple design interations in an efficient manner.

A 3D-printed force sensor was developed by Butzer *et al.* [20] to be compatible with functional magnetic resonance imaging (fMRI). In comparison with other fMRI-compatible force sensors, this 3D-printed device has significantly reduced structure size and manufacturing cost, and achieved relatively high sensing performance. However, because of the drift of this sensor, a calibration is required before every use. Kesner and Howe [21] built up a miniature force sensor utilizing 3DP, and adopted it in a robotic catheter system. This sensor provided relatively high accuracy and robustness to disturbance. However, because of the limitation of its sensing principle employed, further improvement is still needed for enhancing the sensor's measurement resolution and robustness to external noises. An optical force sensor was developed by Nierenberger *et al.* [22]; benefited from the design flexibility of 3DP, it was utilized to manufacturing complex structures that are compatible with harsh environments. However, one drawback of this work is the light reduction of the optical force sensor as a result of volume scattering. On 3D-printed multiaxial force sensors, Kim *et al.* [23] developed a new method to directly fabricate 3D multiaxial force sensor using FDM 3DP of functionalized nanocomposite filaments. Pan *et al.* [24] developed a 3D-printed three-axis micro force sensor and integrated it into a robotic micromanipulation system for measuring the contact force between the tip of an end-effector and a biological sample.

Adopting SLA and FDM-based 3DP techniques, this paper presents the development of two types of strain-gauge micro force sensors with different force ranges and sensing resolutions. A cantilever beam force sensor with a small force range ($\leq$2.5 mN) and high force sensing resolution (4.3 μN) is developed through SLA-based 3DP, and a load-cell force sensor with a large force range ($\leq$120 mN) and medium-level sensing resolution (56 μN) is developed through FDM-based 3DP. Both 3D printers employed are consumer-level, desktop

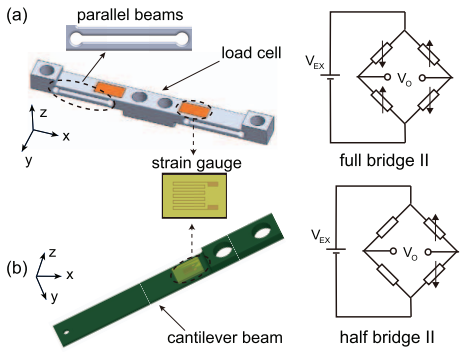

Fig. 1. Design schematics (left) and Wheatstone bridge (right) circuits of (a) load cell sensor and (b) cantilever beam sensor.

models. Finite element analysis (FEA) is performed for design of the force sensing structure, and the ISO 14577 standard is used to accurately calibrate the two sensors.

This paper is the extended version of a previous conference paper [25] that was only focused on the design and calibration of the two 3D-printed micro force sensors. In this version, as proof-of-concept demonstrations of the developed force sensors, we integrate the sensors in customized mechanical characterization systems for measuring the Young's moduli of polydimethylsiloxane (PDMS) samples at different crosslinking levels, and include more technical details, experimental results, and discussions.

II. Sensor Design and Fabrication

A. Design Objectives

In this work, we focused on investigating the limit of structure printing resolution utilizing consumer-level 3D printers, and thus developing 3D-printed force sensors with micronewton resolutions. Moreover, by specifically adjusting the compliance of the sensor structure, we explored the possibility of constructing 3D-printed force sensors with tunable force ranges and sensing resolutions. In order to demonstrate the wide applicability of the proposed force sensing designs and corresponding experimental techniques, we chose two commonly used 3DP techniques (FDM and SLA) and two types of widely-used 3DP filaments (polylactic acid—PLA for FDM and high temperature molding material—HTM 140 for SLA) for sensor structure printing.

The specific design objectives are the following:

- To develop a load cell sensor with a relatively large force range of 0-120 mN and a sensing resolution at the level of 50-100 μN through FDM using PLA filament.
- To develop a cantilever beam sensor with a relatively small force range of 0-2.5 mN and a sensing resolution at the level of 5-10 μN via SLA using HTM 140 filament.

B. Structural Design

Fig. 1(a) shows the structural design of the load cell force sensor. The two groups of parallel-beam flexures (0.8 mm thick for each beam) were designed to tether a central stiff load cell. The parallel beam design constrains potential axial rotations of the central load cell during measurement.

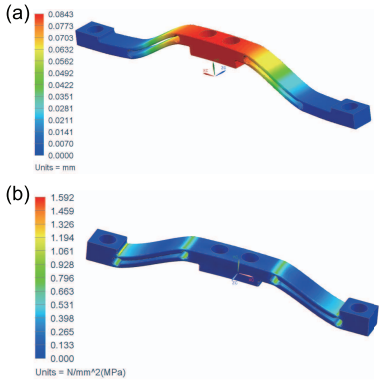

Fig. 2. Finite element analysis (FEA) results of the load cell force sensor structure: (a) displacement distribution and (b) stress distribution.

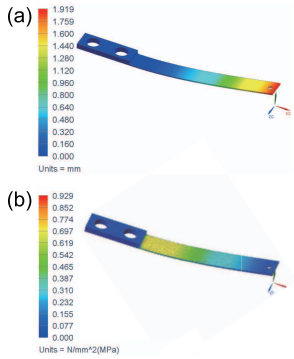

Fig. 3. Finite element analysis (FEA) results of the cantilever beam sensor structure: (a) displacement distribution and (b) stress distribution.

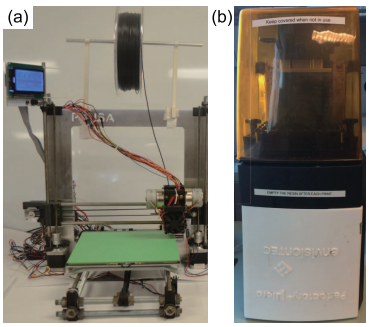

Fig. 4. Photographs of the 3D printers used for sensor structure fabrication: (a) Reprap Prusa I3 and (b) Perfactory Micro EDU.

Mounting holes (diameter: 3.26 mm) are organized in the central load cell and the two stiff ends of the sensor. Holes on the central load cell allow an end-effector to be mounted. At the two ends of the slit between the parallel beams, two strain-concentration holes were arranged to increase the strain at the central ends of the beams. Besides, two holes on the stiff ends of the force sensor were designed for mounting the load cell sensor to the motorized movement stage of a material testing system in order to provide continuous movements during the material testing process.

For structural design of the cantilever beam sensor as shown in Fig. 1(b), the beam dimensions were designed to be 35 mm × 4.5 mm × 0.3 mm (length × width × height), and one small hole (diameter: 1 mm) was designed at the free end of the beam for attachment of an end-effector such as a tiny needle tip (e.g., for force-controlled micromanipulation). Two mounting holes (diameter: 3.26 mm) were designed on the stiff root of the beam to allow the force sensor to be mounted to the material testing system. The connection corner between the beam and its stiff root was designed to be smoothly rounded in order to reduce the risk of beam fracture.

Two factors need to be considered when deciding structural parameters. One issue is to prevent part fracture when specified max force is applied on the sensor, and the other is to design structural dimensions (especially beam thickness) properly to meet the minimal printing resolutions of the 3D printers. Details will be presented in the following sections.

C. Finite Element Simulation

Despite the merits of stress concentration design in the load cell sensor, it may also increase the risk of part fracture. Therefore, finite element analysis (FEA) was conducted to calculate the maximum stress values of both sensors under their maximum loads. Siemens NX software was selected to perform the FEA for the designed sensors. During the FEA, we chose a safety factor of 1.5 and thus applied maximum loads of 180 mN and 3.75 mN to the load cell sensor and the cantilever beam sensor, respectively. Fig. 2 and Fig. 3 show the FEA results of the displacement and stress distribution of the beam structures.

From the FEA results shown in Fig. 2, we can see that, under the maximum load of 180 mN, the load cell sensor generates a maximum deflection of 0.0843 mm [Fig. 2(a)] and a maximum stress of 1.592 MPa [Fig. 2(b)]. The maximum stress and strain (strain distribution not shown) occur at the roots and the central guided ends of the four parallel beams. The polylactic acid (PLA) filament has a yield stress of 62.7 MPa [26], and the max stress value of 1.592 MPa, calculated by the FEA, is well below the material's yield stress. Similarly, from the FEA results shown in Fig. 3, the cantilever beam force sensor generates a maximum deflection of 1.919 mm [Fig. 3(a)] and a maximum stress of 0.929 MPa [Fig. 3(b)]. The maximum stress and strain (strain distribution not shown) occur at the root of the cantilever beam. The maximum stress of the cantilever beam force sensor is also well below the yield stress (56 MPa) of HTM 140. Based on the strain distribution results, the strain gauges will be arranged at the central guided ends of the parallel beams in the load cell structure and at the root of the cantilever beam, maximizing the sensor sensitivity.

D. 3D Printing of Sensor Structures

The 3D printing of the sensor structures is a crucial procedure that will primarily decide the best force sensing resolutions our designs can achieve. Trial-and-error experiments were performed before the best printing resolutions of the two 3DP methods were achieved. The load cell sensor was fabricated by a RepRap Prusa I3 printer [Fig. 4(a)] using

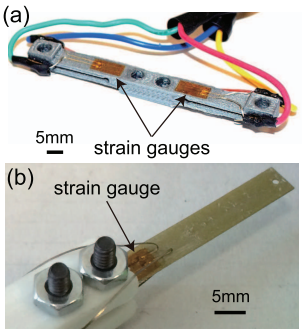

Fig. 5. 3D printed sensors: (a) load cell sensor, (b) cantilever beam sensor.

1.75 mm PLA filaments (ColorFabb). The Prusa I3 printer is based on the FDM technique and has a 0.4 mm nozzle for 1.75 mm filaments, which provides an in-plane printing resolution of 0.4 mm and a vertical printing resolution of 0.2 mm. During printing, one should choose the appropriate orientation for printing based on the designed structures. As supporting material can cause beam thickness variations and leave behind residue that could affect/alter the performance of the load cell, for the printing of our load cell force sensor, in order to avoid the generation of supporting materials in the slits between the parallel beams and four holes going through the load cell, before printing we rotated the 3D model of the load cell along the beam axis [x axis in Fig. 1(a)] by 90°. In order to decrease the stiffness of the load cell and thus generate a higher sensing resolution, we reduced the thickness of the four beams close to the printing resolution. In our selected orientation along which the part will be printed, the major factor affecting the beam thickness is the in-plane printing resolution (0.4 mm). Therefore, we firstly tried to set the thickness of the parallel beams to be 0.4 mm. However, the printing failed because the printed beam was not mechanically stable for successful release, so then we tried to set the thickness to be 0.8 mm, and this time we obtained stable beam structures with the minimal thickness (0.8 mm) the printer could practically print. The 3D-printed load cell sensor is shown in Fig. 5(a). After printing, a fine file was employed to smoothen the beam surface ensuring the areas that the strain gauges (in Section II-E) where placed was flat to get the best possible adhesion. The surface roughness was evaluated to be Ra 10.10 μm using a profilometer (SRG-4000, LabX).

A similar protocol was operated for the printing of the cantilever beam structure. It was fabricated via the SLA technique by a SLA printer [Perfactory Micro EDU; Fig. 4(b)] using HTM 140 resin. This printer is able to produce a higher in-plane resolution (nominal value: 150 μm) and a vertical layer resolution in the range of 50-100 μm. Better surface roughness (Ra 3.25 μm) was obtained due to the higher printing resolution. In our printing, we also rotated the part along x axis [Fig. 1(b)] 90° to make the beam side surface lying on the printing board and avoid supporting material generation in the hole going through cantilever beam. This orientation indicates that the thinnest beam thickness we could print is determined by the in-plane printing resolution (150 μm) of the printer. In the initial trials, we designed our beam thickness to be 0.15 mm. The printing failed because the printed beam composed of only one printed layer that was not mechanically stable. As a result, we further tried to print a beam with a thickness of 0.3 mm, and this time the printed beam was strong enough to sustain applied forces. Fig. 5(b) shows the 3D printed cantilever beam sensor.

E. Signal Readout Electronics

After structural design and FEA of the sensors, it is necessary to implement signal readout electronics on the 3D-printed load cell and cantilever beam to enable force sensing. We selected strain-gauge-based force sensing principle since strain gauges can be easily attached on the 3D printed structures and only involve a simple signal readout circuit (i.e., the Wheatstone bridge circuit). For the load cell sensor, as shown in Fig. 1(a), four strain gauges (Omega, SGD-1.5/120-LY13, 120 Ω) were attached to the top and bottom surfaces of the parallel-beam flexures at their roots, forming a Wheatstone full bridge. The gauges are located at the two central guided ends of the parallel-beam flexures where the maximum strain occurs (Fig. 2(b)). For the cantilever beam force sensor, two strain gauges were attached to the top and bottom surfaces of the cantilever beam and near its root (where the max strain occurs during beam deflection), forming a Wheatstone half bridge with two other 120 Ω fixed-value resistors [Fig. 1(b)]. The excitation voltage for two above Wheatstone bridge is 5 V, and both the full and half bridge circuits can compensate for temperature variations.

Because the output voltage of the Wheatstone bridge circuit is in sub-millivolt level, an amplifier circuit was implemented to amplify the output voltage signal. For the load cell sensor, the output voltage of Wheatstone bridge was measured to be ±0.23 mV at ±180 mN applied force (with the safety factor of 1.5). We adopted a low-noise instrumentation amplifier circuit (INA125P, gain = 5500) to amplify the signal to ±1.27 V at the maximum force, allowing that the load cell can be used in both force directions. Once amplified, the signal needs to be converted into a digital signal so that it can be sent to the host computer. We employed a 24 bit ADC (LTC2440) to convert the analog data into digital format, with the resolution of 0.298 μV. After this conversion, the digital signal was passed into the microcontroller (Arduino Uno) through the SPI (Serial Peripheral Interface) communication. For the cantilever beam sensor, when applying the maximum force of ±3.75 mN (with the safety factor of 1.5) to the sensor tip, the output voltage of Wheatstone bridge was measured to be ± 0.2 mV. A cascade amplifying circuit was built up which consisted of a first-layer amplifier circuit (INA125P, Gain 1 = 504) and a second-layer amplifier circuit (OPA551, Gain 2 = 19.8). The final amplified output voltage is 2 V at the maximum applied force.

To reduce the effect of signal drift, high precision voltage reference (LTC1021-5) was used to supply power to the strain gauges. It is well known that this voltage references has very little drift and will output a constant voltage of 5V. To reduce the effect of electromagnetic interference (EMI) which will get into sensor signal and cause unexpected fluctuations, Faraday cages were built to separate the sensor electronics (Wheatstone bridge circuits and amplifier circuit) from the rest

of the electronics and keep them isolated from external sources of noise. The Faraday cage created a shield of conductive material between the circuit and the external sources. The shield was connected to the electrical ground line to minimize the EMI getting into the sensor electronics and affecting the signal.

III. Sensor Calibration

Once the load cell and cantilever beam sensors were manufactured and the strain gauges were integrated, sensor calibration was performed (3 times for each type, at room temperature ∼23°C and humidity ∼40%) based on the ISO 14577 standard, to obtain the deformation-load data and the output voltage-load data. The former one provides actual quantitative relationship between applied force and resultant deflection, and the latter one is an essential procedure to evaluate the performance (range, resolution, and sensitivity) of the 3D printed force sensor. The ISO 14577 standard specifies that 16 data points are required over the whole measurement range, that three verification deflection measurements are needed, and that the measurement error should be within 2.5%.

A. Load Cell Sensor Calibration

For sensor calibration, the load cell sensor was initially mounted onto a frame through the two side holes, the frame was then placed on a precision balance (Denver Instrument, MXX-123) with a force resolution of 1 μN. A metal rod, firmly mounted on a motorized micromanipulator (MP-285, Sutter), was used to touch the middle part of the load cell sensor and push it vertically. During calibration, the applied force was read directly from the precision balance, and the deflection of the load cell was safely approximated to be the displacement of the micromanipulator (the deformation of metal can be safely neglected because the stiffness of metal rod is estimated to be over 100 times larger than the 3D printed load cell part). In the meanwhile, the output voltage signal of the force sensor was also recorded. The sensor sensitivity can then be calculated as the ratio of output voltage and applied force.

The calibration results of sensor deflection and output voltage as a function of applied force are shown in Fig. 6(a) and 6(b), respectively. From the deflection-force curve, it was derived that the load cell deflection reached 82 μm at the maximum applied force of 180 mN. Compared with simulation result that reveals a maximal deflection of 84.3 μm (Fig. 2(a)), the actual deflection is slightly smaller, which suggests the actual load cell is stiffer than the simulated load cell. Several reasons can justify this small variation. i) Strain gauges were glued to the surface of printed load cell for force sensing. The gluing process holds the strain gauges and printed sensors together once the glue hardens. However, as the beam thickness may somewhat increase after gluing, the beam stiffness will increase accordingly. ii) Unexpected tiny printing errors still exist occasionally due to many issues such as nozzle under/over extrusion, layer separation and splitting, and overheating and vibrations. The induced printing errors made the printed load cell not exactly the same dimension as designed.

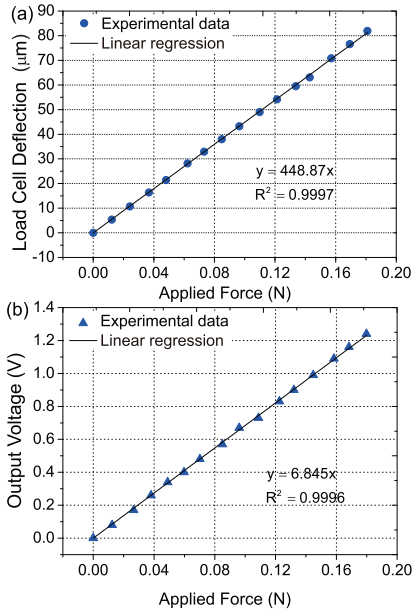

Fig. 6. Calibration results for load cell sensor: (a) deflection calibration and (b) sensitivity calibration.

TABLE I
ISO 14577 Verification for Load Cell Sensor Calibrations

Deflection Calibration		
Actual Deflection (μm)	Sensor Measurement (μm)	Error (%)
78.6	78.75	0.18
67.8	67.36	0.53
35.6	35.50	0.12
Sensitivity Calibration		
Actual Force (N)	Sensor Measurement (N)	Error (%)
0.17625	0.175	0.69
0.09047	0.0909	0.23
0.07841	0.07785	0.31

The output voltage-force curve [Fig. 6(b)] implies that the load cell force sensor is capable of resolving a force up to 180 mN with a sensitivity of 6.845 V/N and a linearity of 1.14%. The force resolution was calculated through measuring standard deviation of the noise level of the output voltage signal, when no load was applied on the force sensor. This noise level was then converted into a force value using the determined sensitivity. Finally, we calculated that the force resolution of the load cell sensor is 56 μN, which satisfies the design specification of 50 to 100 μN. Verification data displayed in Table I indicates that the results of both deflection-force and output voltage-force data satisfy the ISO 14577 standard.

B. Cantilever Beam Sensor Calibration

To calibrate the cantilever beam sensor, the sensor was directly mounted onto the metal rod, and the metal rod was driven by the micromanipulator to move downward and push the precision balance. The applied force, beam deflection and output voltage were recorded simultaneously. The beam sensor deflected 1743 μm at the maximum applied force of 3.75 mN, which is also slightly smaller than the FEA simulation result (1919 μm). This variation can be explained with similar reasons mentioned in load cell sensor calibration.

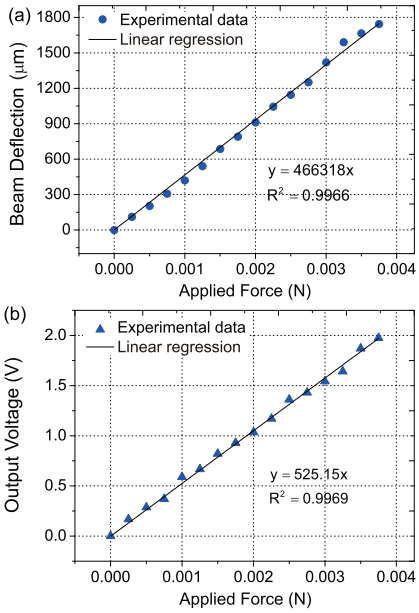

Fig. 7. Calibration results for cantilever beam sensor: (a) deflection calibration and (b) sensitivity calibration.

TABLE II
ISO 14577 VERIFICATION FOR CANTILEVER BEAM SENSOR CALIBRATIONS

Deflection Calibration		
Actual Deflection (μm)	Sensor Measurement (μm)	Error (%)
359.2	372.27	0.75
464.4	473.12	0.5
1208.2	1203.05	0.295
Sensitivity Calibration		
Actual Force (N)	Sensor Measurement (N)	Error (%)
0.00214	0.00209	1.38
0.00284	0.00286	0.52
0.00353	0.00357	1.12

Fig. 7(b) shows the voltage-force calibration curve of the cantilever beam sensor. It is capable of resolving a force up to 3.75 mN with a sensitivity of 525.15 V/N and a linearity of 3.1%. The force resolution was calculated to be 4.3 μN, which meets our design specification of 5-10 μN. Two groups of verification data shown in Table II has verified the accuracy of calibration results.

IV. PROOF-OF-CONCEPT DEMONSTRATIONS

As a proof of concept, we used the two 3D-printed sensors to characterize the mechanical properties of the elastomer PDMS at different cross-linking levels. As the mechanical properties of PDMS have been well characterized [27], we chose it as the testing sample and demonstrate that the 3D printed sensors can be used as effective force sensing components for material mechanical characterization. During the testing, the applied forces were measured by the two sensors, and the materials' Young's moduli were extracted from the measured force-deformation curves.

A. Material Testing Using the Load Cell Sensor

We integrated the load cell force sensor into a custom-made microindenter and performed microindentation testing of the PDMS samples. To prepare the samples, a piece of PDMS (thickness: 4 mm) was prepared using the Sylgard 184 kit (Dow Corning) at three mixing ratios (w/w) of the base to curing agent: 5:1, 10:1, and 20:1. The mixed pre-polymer was poured to a petri dish, degassed in a vacuum chamber for 1 hour, and finally cured at 80°C for 3 hours. A higher mixing ratio of the base to curing agent causes a lower cross-linking level of the PDMS and thus a lower Young's modulus of the cross-linked material.

The load cell force sensor, mounted on a z-axis stage of the microindenter [Fig. 8(a)], was controlled to move vertically at a constant speed, and a spherical indention tip (diameter: 1.5 mm), mounted on the load cell sensor, was used to indenter the PDMS sample. The raw force-deformation data were collected through the data acquisition module of the microindenter. Fig. 8(b) shows three representative force-deformation curves of PDMS samples prepared at the three mixing ratios. Then the raw data were fitted into the following Hertz model to calculate the Young's modulus of the PDMS sample:

$$F = \frac{4}{3} \cdot \frac{E_S \sqrt{R}}{1 - \nu^2} \delta^{\frac{3}{2}} \tag{1}$$

where F and δ are the indentation force and the material deformation, respectively; E_S is the sample Young's modulus, ν is the sample poisson's ratio ($\nu = 0.5$ for PDMS), and R is the radius of the indenter tip.

All the material testing experiments were performed at room temperature (21°C) in ambient environment. Fig. 8(c) shows the measured Young's modulus values of the PDMS samples prepared at the three mixing ratios: 0.81 ± 0.13 MPa (20:1 ratio; n = 5), 3.52 ± 0.56 MPa (10:1 ratio; n = 5), and 4.93 ± 0.31 MPa (5:1 ratio; n = 5). The measured values are comparable to experimental results of the PDMS Young's modulus values previously reported in the literature [28].

B. Material Testing Using the Cantilever Beam Sensor

Besides the indentation-based material testing, we also performed bending tests of PDMS samples to demonstrate the effectiveness of the cantilever beam force sensor. Firstly, PDMS cantilever beams (L = 35 mm, W = 10 mm, H = 3 mm) were fabricated by cutting bulk PDMS with a scalpel. As schematically shown in Fig. 9(a), the cantilever beam sensor was mounted to a metal rod through an adapter passing through the two side holes of the beam. The metal rod was mounted on a micromanipulator and could be controlled to move vertically. The prepared PDMS cantilever beam was firmly clamped on a substrate and placed right underneath the tip of the beam sensor. By driving the sensor to deflect the PDMS sample beam, the force-deformation data of the sample beam was collected and the PDMS Young's modulus values were calculated using the following beam equation:

$$E = \frac{4L^3 F}{\delta W H^3} \tag{2}$$

where E is the Young's modulus of the PDMS beam, F is the applied force to the free end of the beam, L, W, and H are the length, width and thickness of the PDMS beam [Fig. 9(a)], and δ is the deflection of the PDMS beam. The PDMS

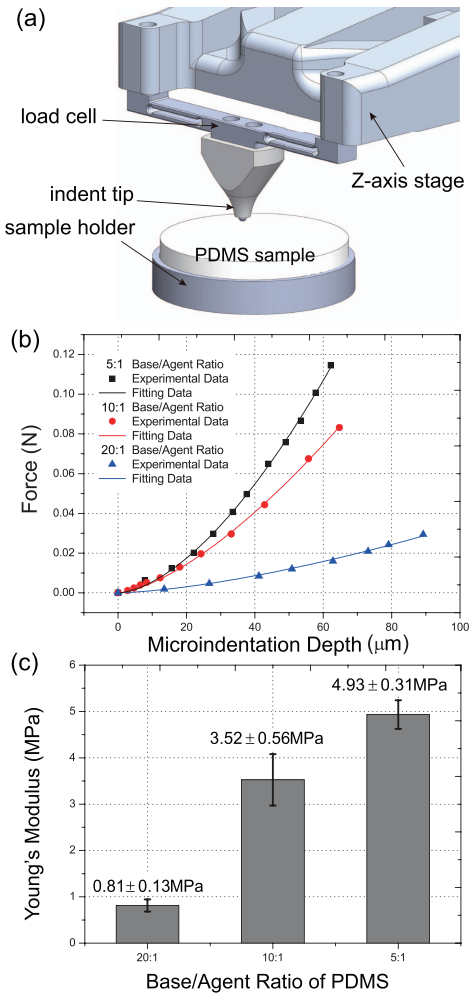

Fig. 8. Experimental demonstration of the load cell force sensor. (a) System setup. (b) Measured force-deformation data at the three mixing ratios. (c) Extracted Young's modulus values (n = 5) of the PDMS samples.

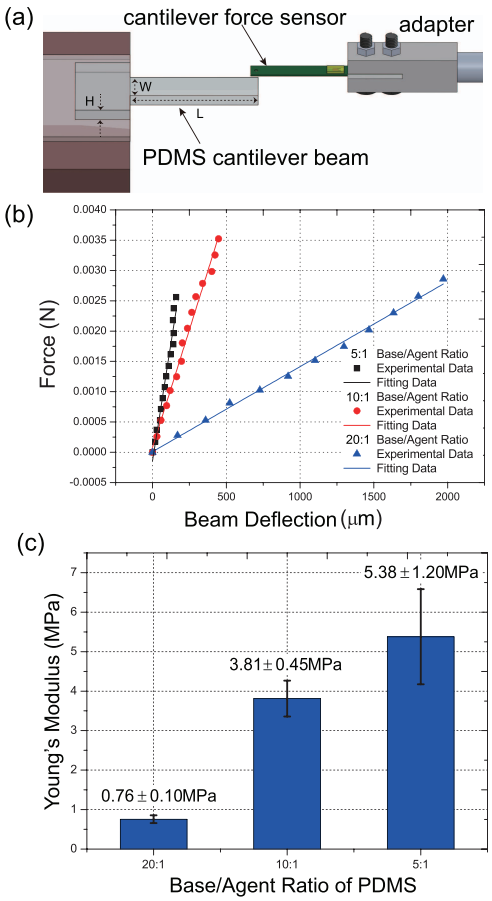

Fig. 9. Experimental demonstration of the cantilever beam sensor. (a) System setup schematic. (b) Measured deflection-force data at 3 mixing ratios. (c) Extracted Young's mudulus values (n = 5) of the PDMS samples.

beam deflection was calculated by subtracting the sensor beam deflection from the total manipulator displacement along the vertical axis. The representative force-deflection curves obtained from the PDMS samples with the three mixing ratios are shown in Fig. 9(b).

As shown in Fig. 9(c), the Young's moduli of PDMS cantilever beam at three mixing ratios were calculated to be 0.76 ± 0.10 MPa (20:1 ratio; n = 5), 3.81 ± 0.45 MPa (10:1 ratio; n = 5), and 5.38 ± 1.20 MPa (5:1 ratio; n = 5). Based on Fig. 8(c) and Fig. 9(c), it is obvious seen that characterization results measured by the cantilever beam sensor are close to those measured by the load cell sensor, which demonstrates the consistent performance and effectiveness of the two force sensors.

C. Discussions

From the sensor development process presented above, several advantages of the developed experimental technique can be summarized as follows:

- It enables rapid prototyping and easy customization of micro force sensors. In the practical 3D printing process of sensor structures, through trial-and-error tuning of sensor structure dimensions, we can investigate the best printing resolutions achievable for generating the best force sensing resolution. Compared with traditional and well-established manufacturing methods, several merits exist for this trial-and-error optimization process, such as the high design flexibility, high time and cost efficiency, and the low material assumption benefited from the additive nature of 3DP.
- The 3DP method for force sensor construction can provide relatively high force sensing resolution at the micronewton level. The 56 μN resolution (comparable with results in [20]–[24]) for the load cell sensor and the 4.3 μN resolution (higher than results in [20]–[24]) for the cantilever beam sensor are of great importance in many types of applications where micronewton-level forces need to be measured, such as micromanipulation, micro-assembly, medical applications, materials science and microdevice calibration. The 4.3 μN resolution we achieved on the cantilever beam sensor is even better than that of a commercial silicon-based piezoresistive force sensor (50 μN) [29].
- The use of non-metal materials (PLA and HTM 140) to fabricate our sensors has also provided several merits such

as light weight, suitability for certain applications (where metal structures are not desired), and the compatibility with corrosive environments where force sensing could be used.

Some limitations still exist in this technique, which can be improved in the future work. Firstly, in case better force sensing resolution is required, more advanced 3D printer (e.g., the two-photon stereolithography based printer [30]) with better printing resolution could be employed. To avoid the potential drawbacks (e.g., delamination, printing errors, time-consuming) induced by the manual gluing attachment of the commercial strain gauges to the printed sensors and make the prototyping more straightforward, direct 3DP techniques of electronic strain-gauges on the sensor structure could be employed in future work, such as the micro-dispensing direct write technology for fabrication of carbon based resistive strain gauge sensor [31] and the embedded 3DP for fabricating strain sensors using gallium-indium alloys [15].

V. Conclusion

This paper presented the development of two 3D-printed strain-gauge micro force sensors with different force ranges and sensing resolution. FEA simulations were performed to evaluate the feasibility of sensor designs, and the 3D printing resolutions of the SLA and FDM methods were experimentally examined to achieve a low sensor structural stiffness. Strain gauges were attached to the 3D-printed sensor structures for force sensing. The developed force sensors are characterized based on the ISO 14577 standard to quantify the sensor accuracy and sensitivity. Two proof-of-concept demonstrations were conducted utilizing the developed force sensors for mechanical characterization of PDMS samples. The Young's modulus results of the PDMS samples, measured by the two force sensors, are in good agreement with each other. The results are also in agreement with previously reported data, demonstrating the effectiveness of the 3D-printed force sensors.

References

[1] S. S. Crump, "Apparatus and method for creating three-dimensional objects," U.S. Patent 5 121 329, Jun. 9, 1992.

[2] C. K. Chua and S. M. Chou, "Rapid prototyping technologies and limitations," *Comput. Aided Integr. Manuf. Systems, Optim. Methods*, vol. 3, pp. 165–185, 2003.

[3] H. Kodama, "Automatic method for fabricating a three-dimensional plastic model with photo-hardening polymer," *Rev. Sci. Instrum.*, vol. 52, no. 11, pp. 1770–1773, 1981.

[4] C. W. Hull, "Apparatus for production of three-dimensional objects by stereolithography," U.S. Patent 4 575 330, Mar. 11, 1986.

[5] R. Sodian *et al.*, "Three-dimensional printing creates models for surgical planning of aortic valve replacement after previous coronary bypass grafting," *Ann. Thoracic Surgery*, vol. 85, no. 6, pp. 2105–2108, Jun. 2008.

[6] G. Cesaretti, E. Dini, X. De Kestelier, V. Colla, and L. Pambaguian, "Building components for an outpost on the lunar soil by means of a novel 3D printing technology," *Acta Astronautica*, vol. 93, pp. 430–450, Jan. 2014.

[7] E. P. Childers, M. O. Wang, M. L. Becker, J. P. Fisher, and D. Dean, "3D printing of resorbable poly(propylene fumarate) tissue engineering scaffolds," *MRS Bull.*, vol. 40, no. 2, pp. 119–126, Feb. 2015.

[8] K. Chizari, M. A. Daoud, A. R. Ravindran, and D. Therriault, "3D printing of highly conductive nanocomposites for the functional optimization of liquid sensors," *Small*, vol. 12, no. 44, pp. 6076–6082, Sep. 2016.

[9] Z. Chen *et al.*, "3D printing of piezoelectric element for energy focusing and ultrasonic sensing," *Nano Energy*, vol. 27, pp. 78–86, Sep. 2016.

[10] M. Vatani, Y. Lu, E. D. Engeberg, and J.-W. Choi, "Combined 3D printing technologies and material for fabrication of tactile sensors," *Int. J. Precis. Eng. Manuf.*, vol. 16, no. 7, pp. 1375–1383, Jun. 2015.

[11] C. L. M. Palenzuela and M. Pumera, "(Bio) Analytical chemistry enabled by 3D printing: Sensors and biosensors," *TrAC Trends Anal. Chem.*, vol. 103, pp. 110–118, Jun. 2018.

[12] K. Willis, E. Brockmeyer, S. Hudson, and I. Poupyrev, "Printed optics: 3D printing of embedded optical elements for interactive devices," in *Proc. 25th Annu. ACM Symp. User Interface Softw. Technol. (UIST)*, 2012, pp. 589–598.

[13] S. J. Leigh, R. J. Bradley, C. P. Purssell, D. R. Billson, and D. A. Hutchins, "A simple, low-cost conductive composite material for 3D printing of electronic sensors," *PLoS ONE*, vol. 7, no. 11, Nov. 2012, Art. no. e49365.

[14] A. Frutiger *et al.*, "Capacitive soft strain sensors via multicore-shell fiber printing," *Adv. Mater.*, vol. 27, no. 15, pp. 2440–2446, Mar. 2015.

[15] J. T. Muth *et al.*, "Embedded 3D printing of strain sensors within highly stretchable elastomers," *Adv. Mater.*, vol. 26, no. 36, pp. 6307–6312, Jun. 2014.

[16] A. Ambrosi and M. Pumera, "3D printing technologies for electrochemical applications," *Chem. Soc. Rev.*, vol. 45, pp. 2740–2755, 2016.

[17] A. D. Valentine *et al.*, "Hybrid 3D printing of soft electronics," *Adv. Mater.*, vol. 29, no. 40, Sep. 2017, Art. no. 1703817.

[18] Y. Wei and Q. Xu, "Design and testing of a new force-sensing cell microinjector based on soft flexure mechanism," *IEEE Sensors J.*, vol. 19, no. 15, pp. 6012–6019, Aug. 2019.

[19] Q. Xu, "Design and development of a novel compliant gripper with integrated position and grasping/interaction force sensing," *IEEE Trans. Autom. Sci. Eng.*, vol. 14, no. 3, pp. 1415–1428, Jul. 2017.

[20] T. Butzer, B. Vigaru, and R. Gassert, "Design and evaluation of a compact, integrated fMRI-compatible force sensor printed by additive manufacturing," in *Proc. IEEE World Haptics Conf. (WHC)*, Jun. 2015, pp. 158–164.

[21] S. B. Kesner and R. D. Howe, "Design principles for rapid prototyping forces sensors using 3-D printing," *IEEE/ASME Trans. Mechatronics*, vol. 16, no. 5, pp. 866–870, Oct. 2011.

[22] M. Nierenberger, S. Lecler, P. Pfeiffer, F. Geiskopf, M. Guilhem, and P. Renaud, "Additive manufacturing of a monolithic optical force sensor based on polarization modulation," *Appl. Opt.*, vol. 54, no. 22, pp. 6912–6918, Jul. 2015.

[23] K. Kim, J. Park, J.-H. Suh, M. Kim, Y. Jeong, and I. Park, "3D printing of multiaxial force sensors using carbon nanotube (CNT)/thermoplastic polyurethane (TPU) filaments," *Sens. Actuators A, Phys.*, vol. 263, pp. 493–500, Aug. 2017.

[24] P. Pan *et al.*, "Robotic stimulation of freely moving drosophila larvae using a 3D-printed micro force sensor," *IEEE Sensors J.*, vol. 19, no. 8, pp. 3165–3173, Apr. 2019.

[25] J. Qu, Q. Wu, T. Clancy, and X. Liu, "Design and calibration of 3D-printed micro force sensors," in *Proc. Int. Conf. Manipulation, Autom. Robot. Small Scales (MARSS)*, Jul. 2016, pp. 1–4.

[26] H. Wang, X. Sun, and P. Seib, "Mechanical properties of poly (lactic acid) and wheat starch blends with methylenediphenyl diisocyanate," *J. Appl. Polym. Sci.*, vol. 84, no. 6, pp. 1257–1262, Feb. 2002.

[27] Y. Xia and G. M. Whitesides, "Soft lithography," *Annu. Rev. Mater. Sci.*, vol. 28, no. 1, pp. 153–184, 1998.

[28] Z. Wang, A. A. Volinsky, and N. D. Gallant, "Crosslinking effect on polydimethylsiloxane elastic modulus measured by custom-built compression instrument," *J. Appl. Polym. Sci.*, vol. 131, no. 22, Jun. 2014, Art. no. 41050.

[29] W. Zhang, X. Dong, and X. Liu, "Switched fuzzy-PD control of contact forces in robotic micromanipulation of drosophila larvae," in *Proc. IEEE Int. Conf. Robot. Autom. (ICRA)*, May 2015, pp. 4080–4085.

[30] F. Niesler and M. Hermatschweiler, "Two-photon polymerization ł A versatile microfabrication tool," *Laser Technik J.*, vol. 12, no. 3, pp. 44–47, 2015.

[31] L.-J. Wei and C. H. Oxley, "Carbon based resistive strain gauge sensor fabricated on titanium using micro-dispensing direct write technology," *Sens. Actuators A, Phys.*, vol. 247, pp. 389–392, Aug. 2016.